Radio Tomographic Imaging with Input Sensor Location Uncertainty

Abhijit Mishra, Upendra Kumar Sahoo and Subrata Maiti.
Department of ECE, National Institute of Technology Rourkela, India

***Abstract*—The device-free localization (DFL) technique for target localization and tracking in a wireless sensor network is important in modern research. Radio tomographic imaging (RTI) is a DFL method that is widely used in today's image-based localization systems. In the RTI system, spatial loss fields (SLFs) represent the maps that indicate the degree of radio wave attenuation for each spatial location in the WSN due to obstacles. In the real-world RTI model, the data is always perturbed by uncertainty. Therefore, uncertainty in sensor node location leads to uncertainty in the input data of the RTI regression model. To address the sensor location uncertainty problem, this paper proposes a novel stochastic robust approximation (SRA) method for RTI (SRA-RTI). Simulation-based performance analysis shows that the proposed technique is robust against the uncertainty in the sensor node location.**

***Index Terms*—Radio tomographic imaging, received signal strength, spatial loss field, stochastic robust approximation.**

I. Introduction

Target localization based on imaging techniques finds extensive application in the modern-day world, ranging from biomedical [1] to military applications. Localization methods are divided into device-based localization and device-free localization. Device-based localization has its limitations in many applications where the object is not directly accessible. This problem does not occur with the DFL technique. One of the DFL techniques is RTI. The RTI method is based on the principle of radio wave absorption by the object present between the transceiver pair [2], [3]. It finds applications like survivor localization after the earthquake, people inside the fire, and surveillance in the border area where privacy is a major concern [4]. Furthermore, RTI has applications related to through-the-wall imaging and survivor localization after earthquakes [2], [3]. Therefore, research in RTI for different environmental situations has attracted the attention of the signal processing community.

RTI uses radio waves to image a specific region of interest within a huge area. The efficacy of RTI lies in the accuracy of the SLF estimation in the region of interest [2].The SLF provides information on the amount of radio frequency (RF) signal power loss between transmitter and receiver due to obstacles in the wireless medium. This information can be obtained by using the received signal strength (RSS) observations at different nodes. Moving objects in the medium contribute to the variance information in the RSS. As the static objects have negligible variance, the shadowing-based RTI (SRTI) is preferred over the variance-based RTI (VRTI) [3]. In SRTI, the attenuation observed due to the obstacles in the medium is the same as the shadowing loss. In SRTI, closer links often experience analogous shadowing [4], [6]. The channel gain between two different points, $\mathbf{P_t} \in \Re^2$ (transmitter position) and $\mathbf{P_r} \in \Re^2$ (receiver position), can be modeled by the following expression:

$$G\left(\mathbf{P_t},\mathbf{P_r}\right) = G\left(\mathbf{P_t}\right) + G\left(\mathbf{P_r}\right) - \beta_0 10\log_{10}\|\mathbf{P_t}-\mathbf{P_r}\|_2 - S\left(\mathbf{P_t},\mathbf{P_r}\right), \tag{1}$$

where $G(\mathbf{P_t})$ (or $G(\mathbf{P_r})$) denotes the power amplifier gain for the transmitter and receiver antennas, respectively. The term β_0 is the path loss exponent, and $S\left(\mathbf{P_t},\mathbf{P_r}\right)$ is the shadowing loss between the transmitter and receiver. If we have information about the transmitter and receiver antenna gains as well as the path loss and shadowing loss, then we can determine the gain between the transceiver pair. The formulation for shadowing loss is as follows:

$$S\left(\mathbf{P_t},\mathbf{P_r}\right) = \int_{\mathcal{A}} w\left(\mathbf{P_t},\mathbf{P_r},\tilde{\mathbf{P}}\right) x\left(\tilde{\mathbf{P}}\right) d\tilde{\mathbf{P}}, \tag{2}$$

where $x : \mathcal{A} \rightarrow \mathbb{R}_+$ is the SLF and the weight function is w. Whereas $x\left(\tilde{\mathbf{P}}\right)$ signifies the extent up to which the radio signal power is absorbed at point $\tilde{\mathbf{P}} \in \mathcal{A}$, and $w\left(\mathbf{P_t},\mathbf{P_r},\tilde{\mathbf{P}}\right)$ provides the contribution of shadowing loss $x\left(\tilde{\mathbf{P}}\right)$ towards the link between $\mathbf{P_t}$ and $\mathbf{P_r}$. Different weight models discussed in [4], [7] were used to assign weight to each pixel of a specific link.

A. Related work and motivation

Most of the research work based on RTI system deal with improving the SLF estimation through some robust models. A one- or two-stage classifier has been proposed in [8] that detects activity between transceiver devices by analysing the impact of environmental changes. A least-square variance-based radio tomography has been proposed in [9] to diminish the impact of intrinsic variations and enhance the localization accuracy of targets in the RTI system. Further, a back-projection-based algorithm has been developed in [10] which reduces the computational cost. This method improves the scalability of the RTI system by compressing the data of a link into a single bit. However, all the above techniques use heuristic weight models. Heuristic weight models have their own limitations in modeling the propagation medium [11]. A kernel-based method has been proposed in [11] to estimate the weight along with the SLF. Furthermore, to deal with the heterogeneous environment, an adaptive Bayesian radio tomography based on a hidden Markov model has been proposed in [12]. A grid-based maximum likelihood

approach has been proposed in [13], which achieves optimal results with low computational complexity. An adaptive RTI system that improves the spatial models through unlabeled data has been proposed in [14]. Here, an on-line technique is also discussed to improve the imaging and estimation of coordinates. A fade-level averaging technique in [15] is used to detect and track multiple objects. This method uses multiple frequencies for each link to aid in multiple target tracking in real-time. Sparsity-based multiple target detection with an energy-efficient DFL technique has been proposed in [16]. This technique is basically used in DFL, where the obstacle is a human being, and a variance-based approach is carried out. Further, the localization accuracy has been increased by the use of a Bayesian grid approach (BGA) in [17]. Here, the prior sensor node location information helps in obtaining the shadowing maps to accurately establish the shadowing effect (the loss occurred due to the obstacles that attenuate the radio signal) of each grid in a link. A generative model is used in building an attenuation image and is proposed in [18] to learn the inherent structure of the SLF. A hierarchic radio imaging (HRI) provides improved localization performance than the BGA and RTI technique was proposed in [19]. Furthermore, the RSS data uncertainty due to quantized RSS for the RTI system has been discussed in [20]. The authors have considered the uncertainty in the RSS or output data of the RTI system due to quantization error.

The research carried out in all the above literature considered the strategic placement of transceiver nodes in the area of interest to achieve higher localization accuracy, which restrains its appropriateness for real-world applications. The above consideration has some practical limitations. Firstly, for a random sensor placement scenario, it is not possible to get the exact sensor node position. A global positioning system needs to be installed on every sensor to get an accurate sensor location, which increases the total cost of the network [21]. A sensor localization algorithm can be used with some anchor nodes to estimate the position of all sensor nodes. These algorithms usually provide the relative or absolute position of the sensor nodes. However, the sensors away from the anchor nodes have more uncertain positions. The criticality of exact placement of sensor nodes along with their practical issues has been discussed in [22]- [23]. In addition to all the stated problems, another important factor that affects the sensor position is physical phenomena like wind, rain, animals, and the movement of soil [24]. Hence, there is always some uncertainty in the sensor node location. Therefore, our objective is to accurately estimate the SLF by considering the uncertainty in the transmitter and receiver nodes. Approaches such as stochastic programming and robust optimization can be used to deal with data uncertainty. It is difficult to fit the uncertain variable probability distribution function (PDF) in stochastic optimization. Therefore, it leads to more computational complexity and issues related to intractability. However, robust optimization (RO) requires the upper and lower bounds for uncertain parameters, which is simpler compared to PDF. Hence, RO provides fewer computations and is more preferred whenever reliability and security are of significance.

This motivates us to develop a robust RTI technique under sensor location uncertainty by using the robust approximation methods [25], [26]. Hence, our contributions are

1) To propose a robust estimator that consider the entire uncertain sensor location region as input for the process of SLF estimation.
2) Regularization based novel robust estimators are proposed based on stochastic approximations to deal with the uncertainty in the input data of the RTI system due to sensor location uncertainty.

This paper is organized in the following manner: The background of RTI and the problem statement are discussed in Section II. The proposed methodology is described in Section III. Simulation-based performance assessment is given in Section IV. Section V contains the conclusion and possible future works.

II. Problem Formulation

Let K wireless sensor nodes be deployed in a convex region of interest $\mathcal{A}$ with a line of sight environment, as shown in Figure 1. All the nodes are equipped with the radio frequency (RF) transceiver unit. Each node can establish $K-1$ number of RF communication links with other nodes. Following the formulation of SRTI [4] and [7], the RSS of a particular link j at time t between the transmitter $k' \in \mathcal{A}$ and receiver $k \in \mathcal{A}$ can be modeled as follows:

$$y_j(t) = P_j(t) - L_j(t) - S_j(t) - F_j(t) - v_j(t), \qquad (3)$$

where, the transmitter power in dB is denoted as $P_j(t)$. The terms $S_j(t)$, $F_j(t)$, $L_j(t)$, and $v_j(t)$ are the shadowing loss, small-scale fading loss, long-distance path loss for the j^{th} link, and measurement noise at the receiver, respectively. Small-scale fading effects can be averaged out by time-averaging the received data. A subspace decomposition technique has been proposed in [9] used to reduce the intrinsic motion. As a result, the fading loss of (3) may be ignored. The distance between the transceiver pair can be used to calculate long-distance path loss provided the exact transceiver position information is available [4]. The path loss of the j^{th} link L_j is related to the and distance between transceiver pair $d_{k',k}$ as:

$$L_j = d_{k',k}^{-\frac{\beta_0}{2}}. \qquad (4)$$

where the path loss exponent is denoted as β_0. For uncertain sensor node positions, we have to find the best possible distance information (optimal distance) between transceiver nodes, as the exact distance information between uncertain transceiver nodes is unknown. This optimal distance helps in obtaining the path loss. With the knowledge of the L_j, P_j can be related to the shadowing loss. Neglecting the fading loss, the equation (3) can be modified as:

$$y_j(t) = P_j(t) - L_j(t) - S_j(t) - v_j(t). \qquad (5)$$

The shadowing loss in (2) can be expressed in discrete form with in M pixels of the RTI network as:

$$S_j(t) = \sum_{m=1}^{M} w_{jm} x_m(t) \quad j = 1, ..., N, \qquad (6)$$

where $x_m(t)$ represents the loss at m^{th} pixel at time t and j is the link index. With this formulation, the SLF to be estimated changes from a function to a vector $\boldsymbol{x} \in \Re^M$. In the non-blind technique [4] and [7], the weighting coefficient w_{jm} is calculated by using the distance between the grid points from the transmitter and receiver positions. If a total of K transceiver nodes are present in region $\mathcal{A}$, then the total number of unidirectional links are $N = \frac{K^2-K}{2}$. w_{jm} in (6) indicates the weight associated with the attenuated pixel m for an unique link j. The normalized elliptical model [5], [20] is the simplest model used in this work to find w_{jm}.

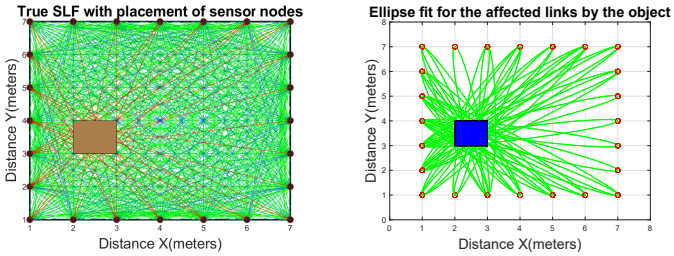

Fig. 1: (a) Deployment of sensors on a square grid. (b) The ellipse fit for affected LOS signals.

To account for static losses (long-distance path loss and fading loss), the RSS difference between time intervals t_a to t_b is taken into account, and thus the difference in RSS values for the j^{th} link can be calculated as Δy_j. The RSS values for all links can be collected into into a matrix and, mathematically, can be represented as below:

$$\Delta \boldsymbol{y} = \mathbf{W}\Delta \boldsymbol{x} + \boldsymbol{v}, \tag{7}$$

where $\Delta \boldsymbol{y} = [\Delta y_1, \Delta y_2, ..., \Delta y_N]^T$, $\Delta \boldsymbol{y} \in \Re^N$ is the difference RSS values, $\Delta \boldsymbol{x} = [\Delta x_1, \Delta x_2, ..., \Delta x_M]^T$, $\boldsymbol{v} = [v_1, ., v_N]^T$, $[\mathbf{W}]_{jm} = w_{jm}$. The noise vector is $\boldsymbol{v} \in \Re^N$, and $\Delta \boldsymbol{x} \in \Re^M$ is the SLF to be estimated , which indicates attenuation due to the obstacles in the WSN. The weight matrix $\mathbf{W} \in \Re^{N \times M}$, where each row represents a weighting towards each pixel for a desired link, and each column represents the weighting of a specific pixel towards all links. To simplify notation, we've replaced $\Delta \boldsymbol{x}$ and $\Delta \boldsymbol{y}$ with $\boldsymbol{x}$ and $\boldsymbol{y}$, respectively. Finding the difference between RSS values using the above-mentioned method is called off-line calibration in SRTI.

Further, the RTI system is an inverse problem, [27] where the cost function can be mathematically represented as:

$$f_{Reg}(\boldsymbol{x}) = f(\boldsymbol{x}) + \lambda h(\boldsymbol{x}). \tag{8}$$

The SLF $\boldsymbol{x}$ is estimated by using the RSS $\boldsymbol{y}$ and the corresponding weight $\mathbf{W}$. The term λ is a tunable parameter that provides appropriate priority to the regularization part $h(\boldsymbol{x})$ over the data fidelity part $f(\boldsymbol{x})$. Different regularization methods are discussed in [4] and [11]. The Tikhonov regularization is the simplest one and can be used for the estimation of SLF $\boldsymbol{x}$. The Tikhonov regularized cost function is given as:

$$f_{Reg}(\boldsymbol{x}) = \frac{1}{2}\|\mathbf{W}\boldsymbol{x} - \boldsymbol{y}\|_2^2 + \lambda \|\mathbf{C}\boldsymbol{x}\|^2, \tag{9}$$

where $\mathbf{C}$ is the smoothing Tikhonov matrix. The optimal SLF $\boldsymbol{x}$ can be calculated using (9) by equating its gradient to zero. Thus, the estimated SLF can be expressed in closed form as:

$$\hat{\boldsymbol{x}} = (\mathbf{W}^T\mathbf{W} + \lambda \mathbf{C}^T\mathbf{C})^{-1}\mathbf{W}^T\boldsymbol{y}. \tag{10}$$

Generally, the SLF does not contain sharp discontinuities, which are basically due to the large operating wavelength compared to objects in the wireless network. Therefore, the SLF can be considered as a Gaussian distribution [4, Equation 3] with certain covariance among the pixels that depends on the distance $d_{m,m'}$ between the pixels m and m'.

$$\mathbf{C}_{\boldsymbol{x}}(d_{m,m'}) = \frac{\sigma_p^2}{k_p} \exp\left(\frac{-d_{m,m'}}{k_p}\right), \tag{11}$$

where k_p is the pixel correlation constant, and it manifests how rapidly the correlation reduces with an increase in distance between pixels. σ_p^2 denotes the shadowing covariance. The inverse of the error covariance matrix $\mathbf{C}_{\boldsymbol{x}}{}^{-1/2} \in \Re^{M \times M}$ is used to estimate the imaging vector.

A. Normalized elliptical weight model

The normalized elliptical weight model [4], [5] can be mathematically expressed as:

$$w_{jm} = \frac{1}{\sqrt{d_{k',k}}} \begin{cases} 1 & \text{if } d_{j,m}(k') + d_{j,m}(k) < d_{k',k} + \Delta \\ 0 & \text{otherwise} \end{cases}, \tag{12}$$

where $d_{k',k}$ is the distance between the transceiver pairs, and $d_{j,m}(k')$ and $d_{j,m}(k)$ are the distances from the centre of a particular pixel m from the transmitter k' and receiver k, associated with a particular link j. The adjustable parameter Δ represents the width of the ellipse. Considering the RTI system under location uncertainty of transceiver nodes, the exact distance information $d_{k',k}$ between transceiver nodes is unknown. Therefore, w_{jm} cannot be evaluated exactly; hence, the sensor node location uncertainty leads to uncertainty in the weight matrix $\mathbf{W}$, which is assumed to be deterministic in earlier literature. Finally, $\mathbf{W}$ becomes a random weight matrix for the uncertain sensor location scenario in the RTI system.

III. Proposed Methodology

In this section, uncertainty in sensor node position is taken into account for the algorithm's development. Our objective is to minimize $\|\mathbf{W}\boldsymbol{x} - \boldsymbol{y}\|_2^2$ while considering a possible variation in the data $\mathbf{W}$ due to the sensor location uncertainty by using robust approximation (RA) techniques such as SRA [26]. The entire uncertain scenario consists of two phases:

1) Design phase.
2) Post-deployment phase.

In the design phase, the sensor locations are obtained by using some localization algorithm. Similarly, there is some sensor location error present due to wild life and rain in the post-deployment scenario [24]. The total uncertainty in sensor location is due to a combination of uncertainty in the design and the post-deployment phase. In the design phase, let a sensor node k be associated with its nominal position (x, y). However, due to the errors introduced in the post-deployment phase, the actual position of k after deployment

is randomly changed to (x_u, y_u) in a deployment region k_u. Here, subscript u indicates the uncertainty in sensor location. As the transceiver node location may take any value in the region k_u which is not exactly known, it is not possible to find the exact distance between the transmitter and receiver.

A. Stochastic robust approximation for RTI (SRA-RTI)

In this technique, the uncertain transceiver region is made discrete, and probabilities are associated with these discrete points. From this, the probability of an uncertain ellipsoid is calculated, and then the sum of the norms problem is formulated. It is assumed that the uncertain region has a Gaussian distribution with a mean (nominal position obtained from the design phase) and standard deviation (maximum uncertainty level). In this model, we have considered some discrete points for the location of the sensor nodes. These points are uniformly presented in the uncertain area, and each point is associated with some probability. Therefore, $\mathbf{W}_i$ can be described as:

$$\mathbf{W}_i = \bar{\mathbf{W}} + \mathbf{U}_i, \quad i = 1, ..., q. \tag{13}$$

Here, $\bar{\mathbf{W}}$ gives the average value of $\mathbf{W}$, and $\mathbf{U}$ characterizes a matrix of independent and identically distributed (IID) Gaussian random variables [25, section 3.4], where the uncertain region is assumed to be Gaussian. For simplicity, we consider the uncertainty in one dimension only. This is explained in Figure 2(a). There are three points in the x-axis direction. The points are $x + \delta$, x, and $x - \delta$. Each point is associated with some probability. The probability is calculated using the probability density function (PDF) of the uncertainty. From Figure 2 the probability of the midpoint is calculated using the integration of the PDF between $(x - \delta/2, x + \delta/2)$. Similarly, the probability for the points $(x - \delta/2, y)$, $(x + \delta/2, y)$ is computed by integrating $(-\infty, x - \delta/2)$, and $(x + \delta/2, \infty)$. Hence, there are three discrete points at the transmitter and receiver uncertain regions.

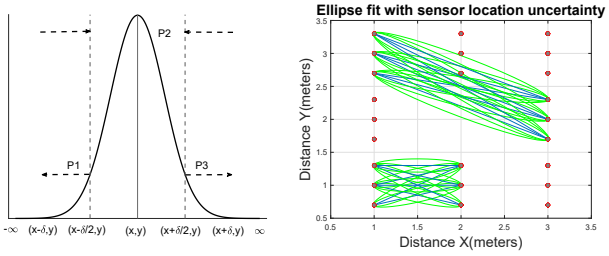

Fig. 2: (a) Gaussian distribution with their probabilities. (b) Position variation of transceiver pairs along with vertical directions.

Figure 2(b) shows that a particular transceiver pair is formed with nine ellipses, each having its own probability. If $p^i_{k'}$ and p^l_k are the probabilities associated with transmitter and receiver points for $i, l = 1, 2, 3$. Let q be the total number of discrete points due to the location change of transceivers along with the true position of transceiver nodes. The probability of the ellipse is calculated by multiplying the probability of the transmitter by the probability of the receiver. Thus, for $q = 9$ ellipses, the probabilities are calculated. Finally, the probability associated with the weight vector for a particular ellipse is found as:

$$p_{il} = p^i_{k'} p^l_k, \tag{14}$$

where p_{il} is the probability associated with a particular ellipse and $p^i_{k'}$ and p^l_k indicate the probability associated with a particular transmitter and receiver point, respectively. In every normal distribution with a specific mean and standard deviation σ, using the empirical rule or 68-95-99.7 rule, about 68% of the data falls within one standard deviation of the mean. The data is 95% within two standard deviations of the mean. As a result, we assign a probability of 1 to the (x, y) positions, 0.25 to the $(x + \delta)$ and $(x - \delta)$positions, and 0.5 to the $\frac{(x+\delta)}{2}$ and $\frac{(x-\delta)}{2}$ points. If we consider the (x, y) points of transmitter and receiver, respectively, then the probability associated with that link is 1, which is the highest among all other combinations. Similarly, if we consider the $(x + \delta)$ and $(x - \delta)$ points of transmitter and receiver, the resulting probability can also be found. If we think of (x, y) points of a particular uncertain transmitter and receiver region, we have the highest probability of 1 multiplied with a link, and for other point pairs of the uncertain regions, we have probabilities of 0.5 and 0.25, respectively. Using this concept, a simple scenario as shown in Figure 2(b) will provide nine probabilities that are associated with the nine weights. From the above analysis, the formulation of the sum of norms becomes

$$\begin{aligned} \boldsymbol{f}(\boldsymbol{x}) = \min_{\boldsymbol{x}} \; & p_1 \left\| \mathbf{W}_1 \boldsymbol{x} - \boldsymbol{y} \right\| + \cdots + p_q \left\| \mathbf{W}_q \boldsymbol{x} - \boldsymbol{y} \right\| \\ & + \lambda \left\| \mathbf{C} \boldsymbol{x} \right\|, \end{aligned} \tag{15}$$

where $\mathbf{C} \in \Re^{M \times M}$ is the smoothing Tikhonov matrix. The above SRA problem can be solved when finite q numbers of $\mathbf{W}$ are considered [26, section 6.4.1]. Hence, $\mathbf{W}_q$ is found for $q = 1, \cdots, 9$. Similarly, $p_1, \cdots, p_q$ is found from (14) for different values of i and l. Hence, the novel **SRA**-RTI formulation can be written as:

$$\begin{aligned} \textbf{minimize} \quad & \boldsymbol{p}^T \boldsymbol{t} + \lambda \boldsymbol{t}_1 \\ \textbf{subject to} \quad & \left\| \mathbf{W}_i \boldsymbol{x} - \boldsymbol{y} \right\| \leq \boldsymbol{t}_i, \; i = 1, \cdots, q, \\ & \left\| \mathbf{C} \boldsymbol{x} \right\| \leq \boldsymbol{t}_1. \end{aligned} \tag{16}$$

Here $\boldsymbol{x} \in \Re^M$ and $\boldsymbol{t} \in \Re^q$ [26, section 6.4.1]. Considering the norm of (16) as the $\boldsymbol{l}_2$-norm, the above problem can be classified as a SOCP problem. Hence, the uncertainty based on SRA can be solved by the sum-of-norms problem using SOCP. The computational cost of SOCP from [28] is given as:

$$\mathcal{O}(\sqrt{L}(m^2 \sum_{i=1}^{L} n_i + \sum_{i=1}^{L} {n_i}^2 + m^3)), \tag{17}$$

where L denotes the SOC constraints, n_i denotes the i^{th} cone dimension, and m represents the equality constraints. The computational complexity of **SRA**-RTI technique is calculated from (17) as $\mathcal{O}(2\sqrt{2}\ M^2)$.

IV. Results and Analysis

For the simulation, a square grid with a 49 m^2 area is used. The sensor nodes are deployed in the monitored area in a regular manner, as shown in Figure 1. The entire monitored

region is divided into discrete pixels, with a side length of 0.2 meters for every pixel. As a result, the monitored area have a total of $M = 900$ spatial positions. The square object is placed at position $[2, 3, 1, 1]$. With $t = 1, 2, \cdots, T$ time instants and $k = 1, 2, \cdots, K$ nodes, we have the training data set $\{x_{u,k}(t), y_{u,k}(t), y_t\}_{t=1}^{T}$. To generate the uncertain sensor position data, the sensor node position is added by some uncertainty parameter, $\mu \in \Re$, with a distribution between [-0.5, 0.5]. The **SRA**-RTI approach estimates SLF based on the uncertain sensor node data.

TABLE I: Parameters of **SRA**-RTI

parameter	Description	Value
K	Number of RF sensor nodes	24
Δ_p	Pixel width (in meter)	0.2
μ	Uncertainty level	[-0.5,0.5]
Δ	Ellipse width (in meter)	0.01
k_p	Constant for correlation between pixel	2.1
σ_p^2	Shadowing covariance of pixel	0.45
λ	Regularization parameter for $\boldsymbol{l}_2$-norm	0.9

The model parameters for normalized ellipse weighting are listed in TABLE I. The regularization constant is selected empirically by finding the average feature similarity (FSIM) for all images at different locations. The regularization constant that corresponds to the highest average FSIM is considered for simulation purposes.

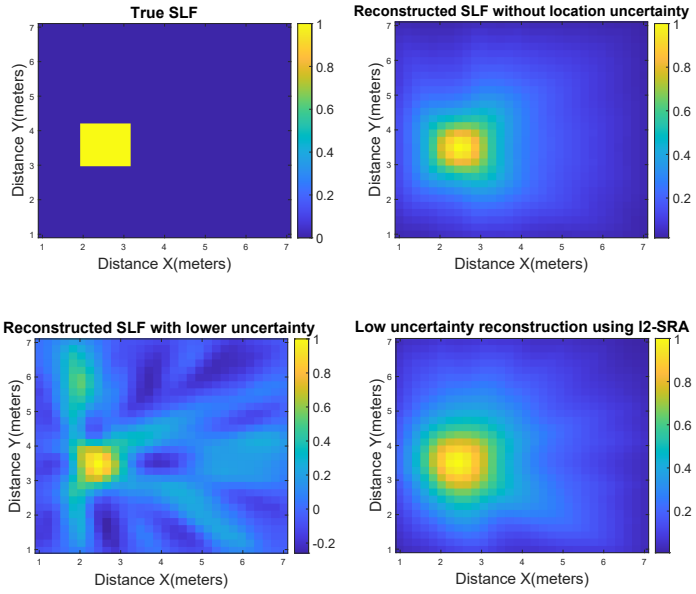

Fig. 3: (a) True SLF, (b) Estimated SLF without uncertainty, (c) Estimated SLF without RA for μ=0.2, (d) Estimated SLF using SRA.

Figure 3 represents the SLF estimation with and without sensor location uncertainty. Figure 3(a) shows the true SLF. Figure 3(b) represents the estimated SLF without location uncertainty by using the Tikhonov regularization technique. In Figure 3(c) shows the output of RTI technique with sensor location uncertainty of μ=0.2m. The poor localization and higher surrounding noise of the estimated SLF are further minimized by using the robust estimator as shown in Figure 3(d). Therefore, comparing 3(c) and 3(d) we verified that **SRA**-RTI outperforms the RTI technique 3(c) with sensor location uncertainty, as can be verified from TABLE II.

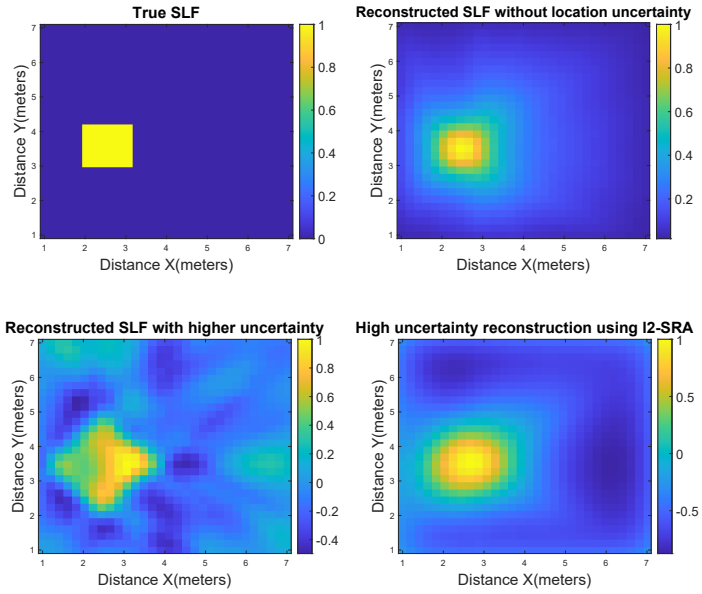

Fig. 4: (a) True SLF (b) Estimated SLF without uncertainty, (c) Estimated SLF without using RA for $\mu = 0.5$ (d) Estimated SLF using SRA.

The performance of **SRA**-RTI technique under higher uncertainty levels is also being investigated. Figure 4(a) represents the true SLF. Figure 4(b) provides the estimated SLF using $\boldsymbol{l}_2$-norm regularization without sensor location uncertainty. A marginal increase in uncertainty level from $\mu = 0.2$ to $\mu = 0.5$ leads to very poor localization of estimated SLF and is verified from Figure 4(c). The reconstructed SLF using **SRA**-RTI is depicted in Figure 4(d). The performance of our proposed technique is almost similar for negative μ values, therefore for simplicity the positive μ values are considered in this work. The quantitative analysis of all findings is shown in TABLES II and III. For quantitative analysis of the estimated SLF using robust techniques under sensor location uncertainty, the following performance metrics [29], [30] are used.

- RMSE (Root mean square error): It is defined as the square root of the mean square error (MSE). Mathematically

$$\textbf{RMSE(dB)} = \sqrt{\textbf{MSE(dB)}}. \tag{18}$$

- SSIM (structural similarity): It indicates the level of degradation in estimated SLF due to structural details change.
- FSIM (feature similarity): It indicates the degree of relatedness among two estimated and actual SLFs based on their features.
- PAR (Pixel attenuation ratio)

$$\text{PAR in } \% = \frac{\text{Number of attenuated pixels}}{\text{Total number of pixels in the object}} \times 100$$

TABLE II: Quantitative analysis of estimated SLF using $\boldsymbol{l}_2$-norm (For lower uncertainty level μ=0.2m)

Parameter	Without uncertainty	Uncertain-RTI	**SRA**-RTI
RMSE in [dB]	-15.60	-7.985	**-14.98**
PAR in %	15.78	28.91	**16.32**
SSIM	0.9121	0.7428	**0.9081**
FSIM	0.9508	0.7915	**0.9497**

TABLE III: Quantitative analysis of estimated SLF using $\boldsymbol{l}_2$-norm (For higher uncertainty level μ=0.5m)

Parameter	Without uncertainty	Uncertain-RTI	**SRA**-RTI
RMSE in [dB]	-15.60	2.429	**-13.05**
PAR in %	15.78	77.36	**27.15**
SSIM	0.9121	0.4285	**0.8864**
FSIM	0.9508	0.5063	**0.9273**

V. Conclusion

In this paper, a robust estimator based on SRA is proposed to handle the sensor node uncertainty for successful estimation of SLF in the RTI system. It is observed that the proposed **SRA**-RTI performs better than traditional RTI with Tikhonov regularization for sensor location uncertainty. **SRA**-RTI results are nearly comparable to SLF estimation performance without sensor location uncertainty. Our technique, on the other hand, employs the $\boldsymbol{l}_2$-norm, which can be applied to other existing regularization techniques to improve performance while also reducing complexity. Furthermore, the proposed technique can be verified by considering real-world RSS values with the help of an actual testbed and should be addressed in the future. The performance of the proposed techniques can be compared for a large monitored region with a varying number of nodes in the future.

References

[1] N. B. Smith and A. Webb, "Introduction to Medical Imaging: Physics, Engineering and Clinical Applications," *Cambridge University Press*, 2010.

[2] N. Patwari and P. Agrawal, "Effects of correlated shadowing: Connectivity, localization, and RF tomography," *In Int. Conf. Info. Process. Sensor Networks, St. Louis, MO*, pp. 82-93, Apr. 2008.

[3] J. Wilson and N. Patwari, "See-through walls: Motion tracking using variance-based radio tomography networks," *IEEE Trans. Mobile Comput.*, vol. 10, no. 5, pp. 612-621, May. 2011.

[4] B. R. Hamilton, X. Ma, R. J. Baxley, and S. M. Matechik, "Propagation modeling for radio frequency tomography in wireless networks," *IEEE Journal of Selected Topics in Signal Processing.*, vol. 8, no. 1, pp. 55-65, Feb. 2014.

[5] J. Wilson and N. Patwari, "Regularization methods for Radio Tomographic Imaging," *in Virginia Tech Symp. Wireless Personal Commun.*, Aug. 2009.

[6] J. Wilson and N. Patwari, "Radio tomographic imaging with wireless networks," *IEEE Trans. Mobile Comput.*, vol. 9, no. 5, pp. 621-632, 2010.

[7] Wilson, Joey and Patwari, Neal and Vasquez, Fernando Guevara, "Regularization methods for radio tomographic imaging," *2009 Virginia Tech Symposium on Wireless Personal Communications*, 2009.

[8] S. Sigg, M. Scholz, S. Shi, Y. Ji, and M. Beigl, "RF-sensing of activities from non-cooperative subjects in device-free recognition systems using ambient and local signals," *IEEE Transactions on Mobile Computing*, vol. 13, no. 4, pp. 907-920, 2014.

[9] Y. Zhao and N. Patwari, "Robust estimators for variance-based devicefree localization and tracking," *IEEE Transactions on Mobile Computing*, vol. 14, no. 10, pp. 2116-2129, Oct. 2015.

[10] Huseyin Yi gitler, Riku J antti, Ossi Kaltiokallio, and Neal Patwari, "Detector Based Radio Tomographic Imaging," *IEEE Transactions on Mobile Computing*, vol. 17, no. 1, pp. 58-71, Jan. 1 2018.

[11] D. Romero, D. Lee and G. B. Giannakis,"Blind Radio Tomography," *in IEEE Transactions on Signal Processing* , vol. 66, no. 8, pp. 2055-2069, April 15, 2018.

[12] D. Lee, D. Berberidis, and G. B. Giannakis, "Adaptive Bayesian radio tomography," *IEEE Transactions on Signal Processing*, vol. 67, no. 8, pp. 1964-1977, 2019.

[13] Z. Wang, H. Liu, S. Xu, X. Bu, and J. An, "Bayesian device-free localization and tracking in a binary RF sensor network," *Sensors*, vol. 17, no. 5, 2017.

[14] Ossi Kaltiokallio, Riku Jantti , and Neal Patwari, "ARTI: An Adaptive Radio Tomographic Imaging System," *IEEE Transactions on Vehicular Technology*, vol. 66, no. 8, pp. 7302-7316, Aug. 2017.

[15] M. Bocca, O. Kaltiokallio, N. Patwari, and S. Venkatasubramanian, "Multiple target tracking with RF sensor networks," *IEEE Transactions on Mobile Computing*, Vol. 13, pp. 1787-1800, 2014

[16] J. Wang et al., "E-HIPA: An energy-efficient framework for high precision multi-target-adaptive device-free localization," *IEEE Trans. Mobile Comput.*, vol. 16, no. 3, pp. 716-729, Mar. 2017.

[17] J. Wang, Q. Gao, P. Cheng, Y. Yu, K. Xin, and H. Wang, "Lightweight robust device-free localization in wireless networks," *IEEE Trans. Ind. Electron.*, vol. 61, no. 10, pp. 5681-5689 , Oct. 2014.

[18] Zhongping Cao, Zhen Wang, Hanting Fei, Xuemei Guo, and Guoli Wang, "Generative model based attenuation image recovery for device-free localization with radio tomographic imaging," *Pervasive and Mobile Computing*, vol. 66, pp. 101-205, 2020.

[19] Ding, Xuejun and Choi, Tsan-Ming and Tian, Yong, "HRI: Hierarchic Radio Imaging-Based Device-Free Localization," *IEEE Transactions on Systems, Man, and Cybernetics: Systems*, vol. 52, no. 1, pp. 287-300, 2022.

[20] Mishra, Abhijit and Sahoo, Upendra Kumar and Maiti, Subrata,"Sparsity-enabled radio tomographic imaging using quantized received signal strength observations,"*Digital Signal Processing* , vol. 127, pp. 103576, 2022.

[21] N. Patwari, "Location Estimation in Sensor Networks. PhD Thesis," *University of Michigan, Ann Arbor, MI, USA*, 2005.

[22] Prasithsangaree, P. and Krishnamurthy, P. and Chrysanthis, P., "On indoor position location with wireless LANs," *The 13th IEEE International Symposium on Personal, Indoor and Mobile Radio Communications*, vol. 2, pp. 720-724, 2002.

[23] Sanay Abdollahzadeh and Nima Jafari Navimipour, "Deployment strategies in the wireless sensor network: A comprehensive review," *Computer Communications*, vol. 91-92, pp. 1-16, 2016.

[24] Shazly, Mohamed H. and Elmallah, Ehab S. and Harms, Janelle, "Location Uncertainty and Target Coverage in Wireless Sensor Networks Deployment," *IEEE International Conference on Distributed Computing in Sensor Systems*, pp. 20-27, 2013.

[25] John C. Duchi,"Optimization with uncertain data," *Stanford University Press*, May 29, 2018.

[26] S. Boyd and L. Vandenberghe,"Convex Optimization," *Cambridge University Press*, 2004.

[27] P. C. Hansen,"Discrete inverse problems: insight and algorithms," *SIAM*, 2010.

[28] Plik, I., and Terlaky, T.,"Interior Point Methods for Nonlinear Optimization.," *In Nonlinear Optimization, 1st ed.; Di Pillo, G., Schoen, F., Eds.; Springer Berlin Heidelberg: Cetraro, Italy,*, 2010.

[29] U. Sara, M. Akter, and M. S. Uddin, "Image quality assessment through fsim, ssim, mse and psnr comparative study," *Journal of Computer and Communications*, vol. 7, no. 3, pp. 818, 2019.

[30] Mishra, Abhijit and Sahoo, Upendra Kumar and Maiti, Subrata, "Distributed Incremental Strategy for Radio Tomographic Imaging," *2020 IEEE 17th India Council International Conference (INDICON)*, pp. 1-6, 2020.

[31] Mishra, Abhijit and Sahoo, Upendra Kumar and Maiti, Subrata,"Sparsity based Radio Tomographic Imaging using Fused Lasso Regularization," *Advanced Communication Technologies and Signal Processing (ACTS)*, pp. 1-6, 2021.